Landslides (2020) 17:2189–2203
DOI 10.1007/s10346-020-01436-0
Received: 18 January 2020
Accepted: 5 May 2020
Published online: 7 June 2020

Yanbo Zhang · Aiguo Xing · Kaiping Jin · Yu Zhuang · Muhammad Bilal · Shimin Xu · Yaoqiang Zhu

Investigation and dynamic analyses of rockslide-induced debris avalanche in Shuicheng, Guizhou, China

Abstract On July 23, 2019, a large catastrophic landslide occurred in Shuicheng, Guizhou, China. It was a rapid and long run-out landslide that resulted in more than 50 casualties. The displaced materials traveled an approximate distance of 1250 m, with a descending height of around 465 m. In this paper, seismic record analyses and numerical simulation were conducted to determine the run-out behavior of the Shuicheng landslide. To determine the main characteristics of the landslide, geological and climatic settings were obtained by conducting a detailed field survey. The DAN3D model was used to simulate the propagation and run-out process of the landslide. It was observed that a combined Frictional-Voellmy model provides assuring results in simulating the Shuicheng landslide. The total duration of the landslide is 60 s with an average velocity of 20 m/s. The maximum velocity is estimated to be 40 m/s along the right bank of the valley, while a high initial velocity of 24 m/s was recorded at the initiation of the landslide. Seismic records obtained from the nearby seismic stations were used to calculate the location of the event and interpret the dynamic process of the landslide. The Arias intensity, Hilbert-Huang transform, and Empirical mode decomposition were used to obtain a detailed time history of the landslide. The results of the numerical simulation and seismic record analyses are expected to portray the process of similar landslides. This will improve the accuracy of landslide hazard mapping in the region.

Keywords Shuicheng landslide · Numerical simulation · DAN3D · Seismic records

Introduction

In southwest China, especially in Guizhou province, karst is the dominant geological feature. In the past few decades, this region has been subjected to catastrophic long-runout landslides triggered by earthquakes, heavy rainfall, and human activities (Chigira et al. 2010; Xu et al. 2010; Yin and Xing 2012; Xing et al. 2015, 2016; Li et al. 2017). On July 23, 2019, at 8:40 p.m., a massive landslide occurred in Shuicheng, Guizhou, China, resulting in more than 50 casualties as well as a massive loss to infrastructure in that area. The pre- and post-event images are shown in Fig. 1.

Distinctive efforts have been made to prevent and mitigate such kind of landslide hazard, and there is a significant reduction in the casualties caused by these disasters. To better understand the mechanisms involved in landslides, various methods are being used to analyze or simulate landslides, including seismic records, numerical simulation, and video records. Video records are the most perceptual method, but it is difficult to obtain, especially in remote areas (Zhu et al. 2019). In this paper, seismic record analyses and numerical simulation were conducted. Furthermore, their comparative analyses were done to determine the run-out behavior of the Shuicheng landslide.

Large landslides can generate seismic waves strong enough to be visible above the noise level that can be recorded by the seismic stations locally, even globally (Yamada et al. 2013). By comparing the analyses of the seismic records with the video record, the results indicate that each impact of the rockfall along the run-out path produces strong P-waves (Vilajosana et al. 2008). Many studies have been performed through seismic records, and different methods have been proposed to detect, locate, and monitor landslides through analyses of seismic records (Navarre et al. 2009; van Herwijnen and Schweizer 2011b; Van Herwijnen and Schweizer 2011a; Leprettre et al. 1996; Leprettre et al. 1998; Helmstetter and Garambois 2010). It is noted that machine learning method was used to develop a pattern recognition to detect avalanche from passive seismic data (Rubin et al. 2012).

Due to its unique ability to collect information, seismic records are widely used to interpret the process during landslides with a small time duration. Combining the seismic record analyses with field investigation, a detailed time history of the mass movement can be resolved (Allstadt 2013; Yamada et al. 2013; Moretti et al. 2015; Bai et al. 2019; Coe et al. 2016; Moran et al. 2008; Ward and Day 2006).

Numerical studies have been carried out to obtain a better understanding about the hypermobility of landslides, and some rational methods have been proposed to predict run-out behavior of landslides (Sassa 1988; Pastor et al. 2002, 2009, 2018; McDougall and Hungr 2004, 2005; Hungr and McDougall 2009; Hungr 1995; Denlinger and Iverson 2004; Cascini et al. 2016). Many studies have validated these methods through back analyses (Quan Luna et al. 2016; Liu et al. 2015; Dai et al. 2016).

In this paper, a thorough field survey was conducted to obtain the geological and climatic setting of the Shuicheng landslide and determine its main characteristics. The dynamic DAN3D model was used to simulate the run-out behavior of the landslide. For numerical analyses of the Shuicheng landslide, the most suitable rheological models and parameters were calibrated and validated according to the results of field investigation and seismic records. In addition, seismic records were analyzed to determine the location and the process of the Shuicheng landslide, and the results were compared with the numerical analyses. The results of the numerical simulation and seismic record analyses are expected to portray the process of a similar landslide in a better way, and hence improve the accuracy of landslide hazard mapping in the region.

Geological and climatic setting

The study area is located in the middle mountain-plain of the central part of Guizhou. The elevation ranges from 1180 to 2070 m at the bottom to top of the mountain, while the source area is at an elevation of 1658 m. There is an elevation difference of 890 m, and the average angle of the side slope is around 24°. The pre-event location of the Shuicheng landslide is shown in Fig. 2(a).

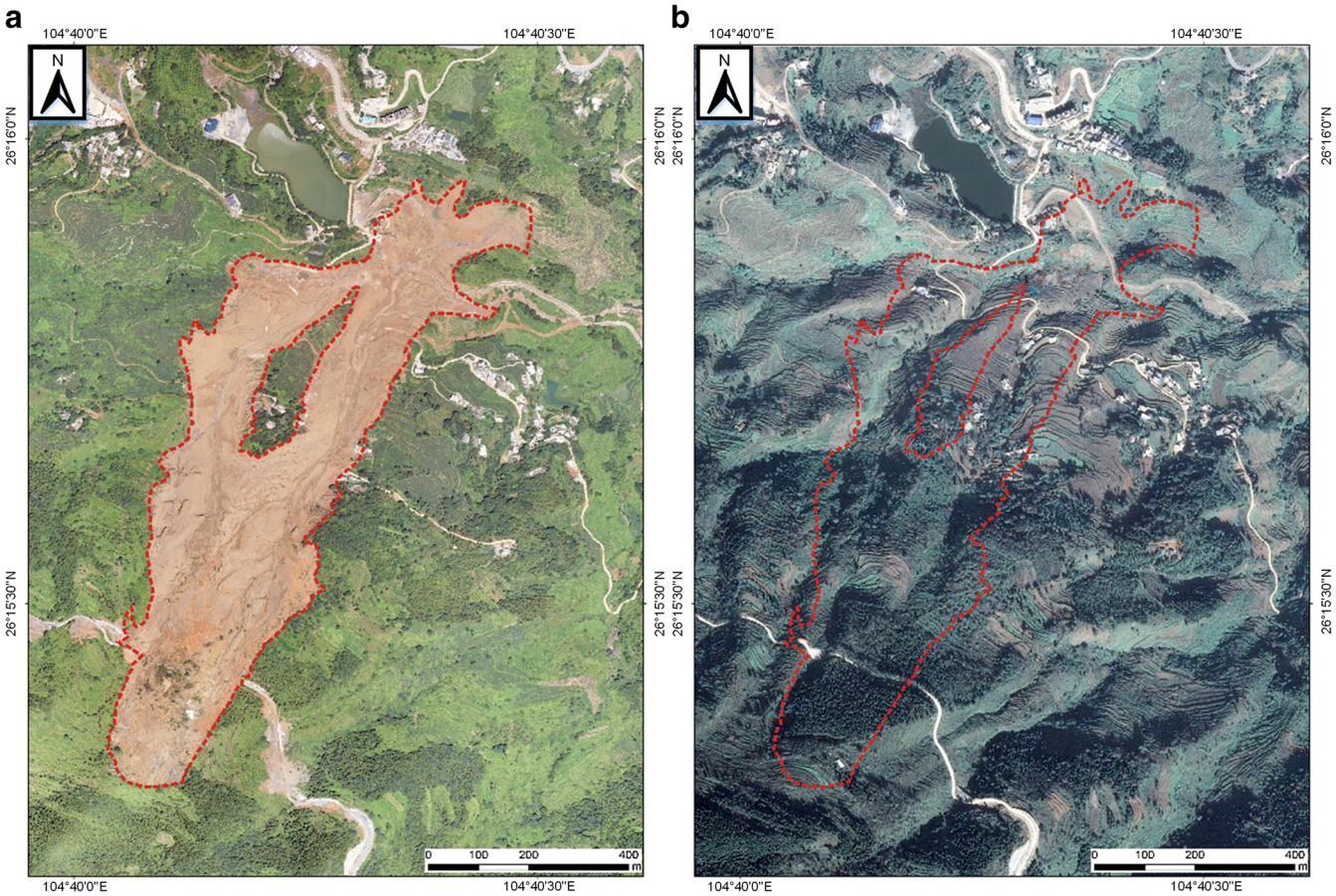

Fig. 1 **a** Pre-event image of the Shuicheng landslide. **b** Post-event image of the Shuicheng landslide

There were two pre-event valleys shown in Fig. 2(b), providing the sliding mass with separate distinctive paths.

The exposed rocks in the study area range in age from Permian to Quaternary. It includes the Feixianguan Group sandstone and mudstone (T_1f) of Early Triassic, the Xuanwei Formation (P_3x), the Emei Mountain basalt ($P_2\beta$) of Middle Permian, and Quaternary deposits ($Q_4al + pl$) with a thickness of 0 to 20 m (Fig. 3). The landslide mainly occurred in the Emei Mountain basalt of Middle Permian.

The study area is located in the Yangzi Platform. The basic structural framework of the study area was formed due to the Yanshan tectonic uplift at the end of the Late Mesozoic Era and the regional plateau resulted from peneplanation by the end of the Miocene. Joints and fractures are extremely developed in the study area. The majority of the mountains in this area are distributed along the geological structure line that develops into deep, long, and V-shaped valleys. Furthermore, the undulations in the terrains are more organized in a parallel comb arrangement; landform erosion, dissolution-landform erosion, and karst landform are relatively more developed.

The study area has a plateau monsoon climate, with mild temperature and abundant rainfall. According to the data from the Meteorological Bureau of Guizhou province, the annual average temperature ranges from 11 to 17 °C. The annual average rainfall ranges from 940 to 1450 mm, primary precipitation occurs during the monsoon season which lasts from June to August. An intermittent rainfall occurred in Shuicheng county from June 1 till the evening of the event (July 23). From June 23 to July 23, the accumulated rainfall in the study area was 369.2 mm, of which the continuous heavy rainfall from July 18 to July 23 accumulated 287.1 mm. The rainfall recorded on July 22 was up to 98 mm. There were three heavy rainfall spells in Shuicheng county, just before the landslide event. These sessions occurred on the night of July 18, from the night of July 19 to 20, and on the night of July 22.

The groundwater in the study area can be divided into two types: fissure water in basalt and pore water in loose Quaternary deposits. The Quaternary deposits are mostly comprised of silty clay, which has a medium permeability. The pore water in the quaternary silty clay was mainly recharged from atmospheric precipitation. Due to the overtime development of the basalt joint fissures, a high yield of water fills the joint fissures in the basalt layer of the bedrock.

Shuicheng landslide

The Shuicheng landslide involved a total volume of 2 Mm^3, including 1.6 Mm^3 of jointed basaltic rock mass from the source area and 0.4 Mm^3 of material entrained during transport. The Shuicheng landslide can be divided into three zones based on the

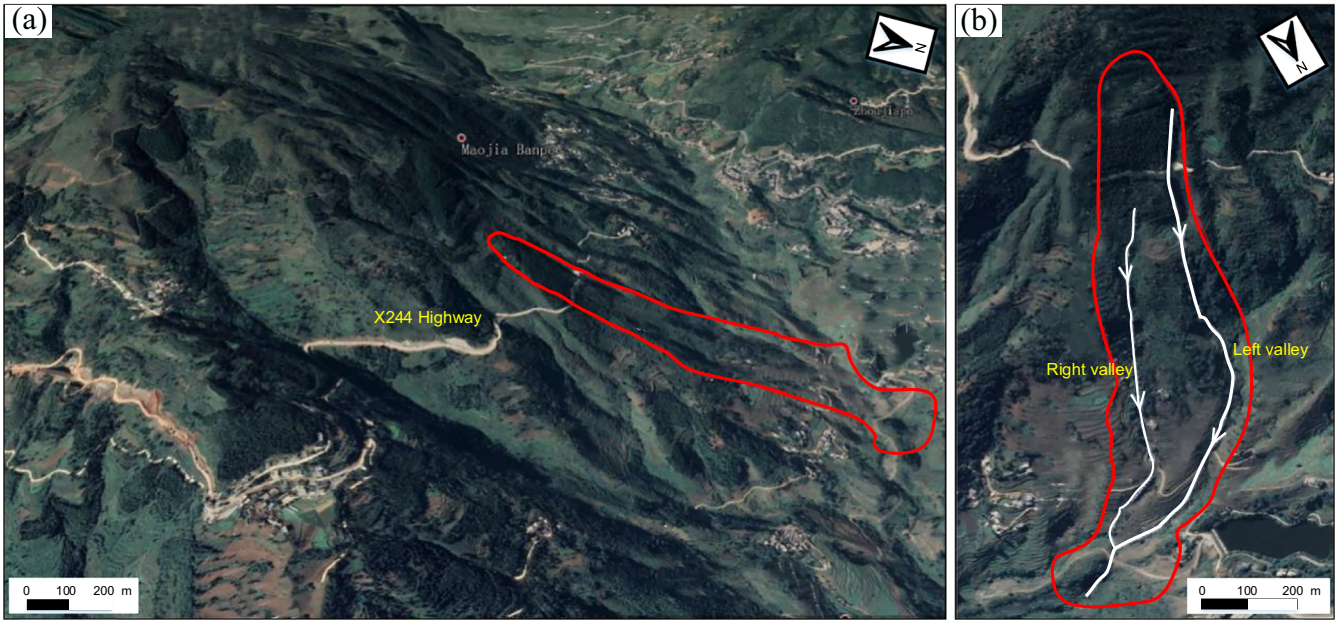

Fig. 2 **a** Pre-event location of the Shuicheng landslide. **b** Pre-event image of the two valleys

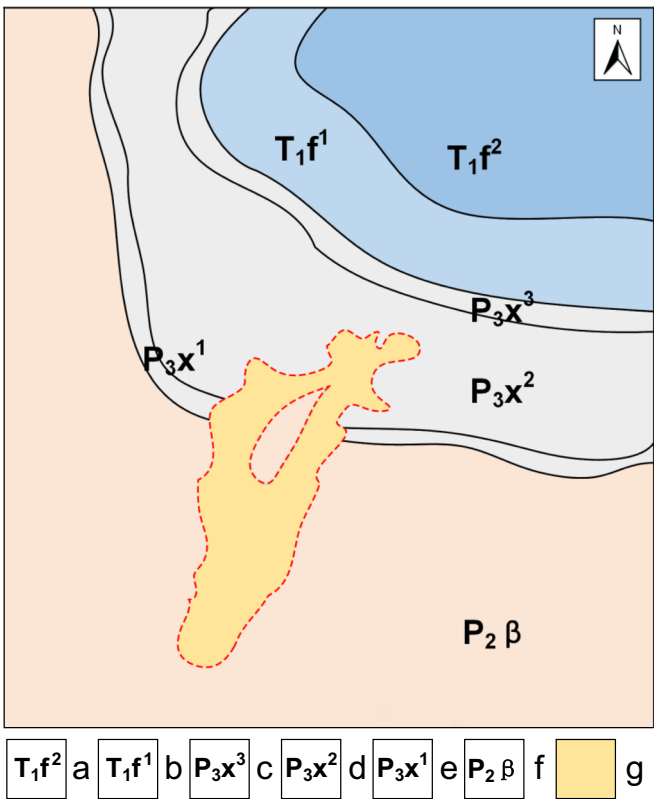

Fig. 3 Geological map of the Shuicheng landslide. **a**: Second part of Feixianguan Formation, Lower Triassic; **b**: first part of Feixianguan Formation, Lower Triassic; **c**: third part of Xuanwei Formation, Upper Permian; **d**: second part of Xuanwei Formation, Upper Permian; **e**: first part of Xuanwei Formation, Upper Permian; **f**: Permian basalt; **g**: landslide area

field survey, namely source area, entrainment area, and deposition area.

Based on the field survey, a 3D sketch of the post-event Shuicheng landslide is presented in Fig. 4. The landslide dropped approximately 465 m in elevation and extended about 1250 m from the head scarp to the distal edge of the landslide toe. The landslide initiated as a rock slide in the large basalt rock mass with a strike angle of 20° to 26° and a dip of 50°, respectively. After detaching from its source area, the slide mass ran down rapidly. The displaced material was divided into two branches due to a collision with a basaltic ridge (Fig. 5) at an elevation of 1450 m. The separated sliding mass continued to travel along both banks of the valley, entraining sediments in the run-out path. At the deposition area, both branches of the displaced mass once again merged into each other.

The source area is located in the upper part of the roadway X244 at an elevation ranging from 1518 to 1658 m. The toe of the rupture surface is approximately located at an elevation of 1515 m. Before the landslide event, a house was located near the head scarp of the source area. When the moving mass detached, it also carried that house along with it. After covering a short distance, the remains of it were distributed along the run-out path. It can be determined by the remains of the house that the slope angle of the source area is approximately 50°. The source area has an estimated volume of 1.6 Mm^3 and an average thickness of 20 m. After the event, three major joints sets are presented in the rear of the source area at 160°/26°, 300°–305°/50°–55°, and 136°/69°.

The entrainment area is located at a relief ridge at an elevation ranging from 1182 to 1518 m. The average slope angle of the entrainment area is around 35°. Two natural valleys surround the basaltic ridge (Fig. 5) provided the moving mass with two entrainment run-out paths. The right valley has a width of 130 to 150 m, and the left valley has a width of 140 to 170 m. Approximately 0.4

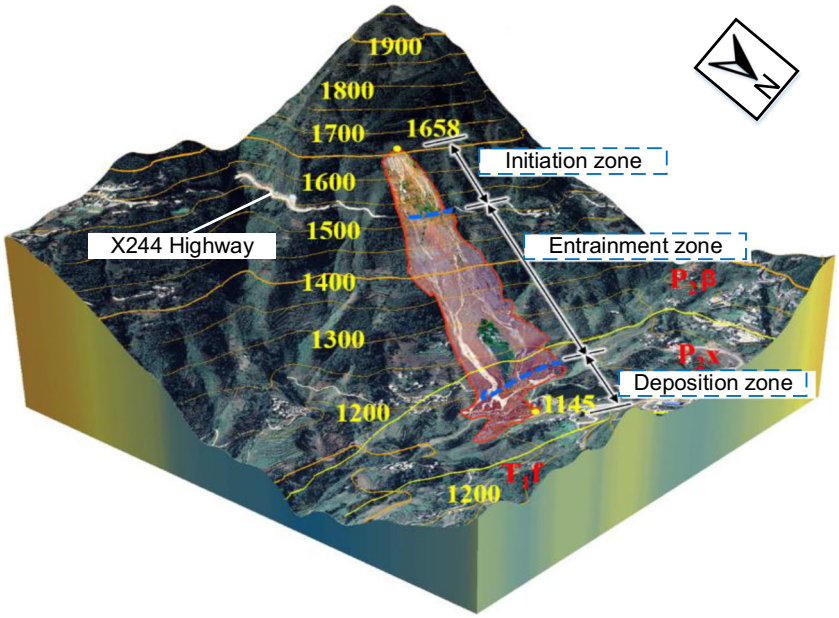

Fig. 4 Three-dimensional image of Shuicheng landslide

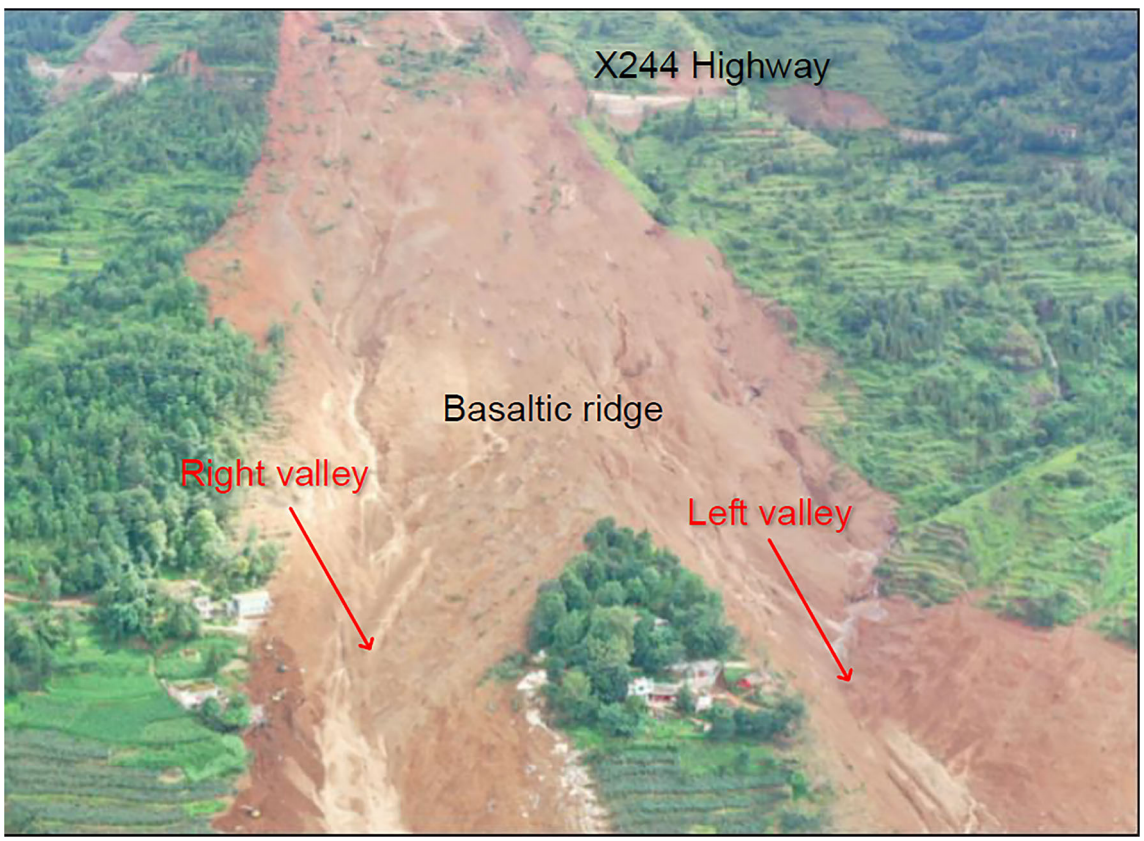

Fig. 5 UAV image of basaltic ridge

Mm^3 of loose deposits was eroded and entrained during emplacement.

The deposition area is located at an elevation ranging from 1180 to 1200 m with an average slope angle of 0 to 10°. The displaced material was mainly deposited in the middle part of the deposition area due to the two branches of the moving mass collided with each other. It is estimated that the displaced material has a volume of 1.37 Mm^3 by a comparison of pre- and post-event DEMs.

Another important thing to mention is that there were a lot of human engineering activities near the source area before the event. In November 2018, there was a widening of the X244 highway. Also, in July 2019, excavation works were carried out on the X244 highway. Those human activities could be one of the triggering factors of the landslide. InSAR was used to monitor the deformation of the X244 highway. From May 26 to July 7, 2019, InSAR results reveal no obvious deformation, which was further validated by the field survey. Hence, human activities are one of the factors triggering the landslide.

Numerical analyses

Dynamic model and parameters

In this paper, a dynamic model DAN3D, developed by Hungr and his colleagues (McDougall and Hungr 2004, 2005; Hungr et al. 2005), was used to simulate and analyze the behavior of the Shuicheng landslide. Based on smoothed particle hydrodynamics (SPH), the numerical model is used for the dynamic analyses of rapid flow slides, debris flows, and avalanches. To simulate different types of rapid landslides involving different geological materials, various kinds of basal rheological relationships were implemented in DAN3D, including the frictional and Voellmy model.

The frictional rheology assumes the resisting shear force (τ) to depend only on the effective normal stress (σ). The governing equation of the frictional rheology is expressed as:

$$\tau = \sigma(1-r_u)\tan\phi \quad (1)$$

where the pore pressure ratio, r_u, and the dynamic basal friction angle, ϕ, are the rheological parameters of the frictional model.

The Voellmy rheology combines frictional and turbulent behaviors:

$$\tau = \sigma f + \rho g v^2/\xi \quad (2)$$

where the friction coefficient, f correlates the shear stress with the normal stress, and the turbulence coefficient summarizes all the velocity-dependent factors related to the flow resistance.

However, the controlling process of the Shuicheng landslide is too complex to select an appropriate method beforehand. Frictional-Voellmy combined model has been found the most accurate basal rheologies through a trial-and-error procedure. The frictional model was employed in the source area, and the Voellmy model was used to simulate the behavior of entrainment and deposition material. The source area, entrainment, and deposition areas are displayed in Fig.6.

Back-analyses were performed to determine the most suitable rheological parameters for the simulation (Cuomo et al. 2016). A friction angle of 24° and a pore pressure ratio of 0.4 were selected for the frictional model. In the Voellmy model, a frictional coefficient of 0.2 and a turbulence coefficient of 900 m/s^2 were adopted for the entrainment and deposition areas. Detailed rheological parameters are presented in Table 1.

Simulated results

The results of the DAN3D simulation are presented in Fig. 7. The depth distribution at different time steps was plotted at 6-m intervals. The duration of the movement lasted approximately 60 s with only lateral expansion occurring in the following time. The final distribution of the deposited sliding mass ranges from 2 to 24 m, with the maximum thickness located at the end of the left valley.

On the basis of the field survey, the results of the simulation are thus consistent with the actual event in terms of the run-out distance and deposit distribution. At 15 s, the front edge of the slide mass collided with a dense and stable basaltic ridge at an elevation of 1450 m. Then the moving mass divided into two debris avalanche and moved forward along the valleys surrounding the basaltic ridge. The sliding mass moved entirely out of the source area in approximately 20 s, which is consistent with the result of the seismic signals. According to the maximum velocity image (Fig. 8), the mass moving on the right valley reached the deposition area first because the velocity of the right branch of the moving mass was higher than the left one. Both branches of the moving mass collided and merged into each other and gradually stopped at the deposition area.

The plot of maximum velocity versus running distance is shown in Fig. 8. A high velocity of 24 m/s was recorded at the initial stage of the landslide. The maximum velocity is estimated at around 40 m/s at the right bank of the valley.

To further understand the erosion depth of the Shuicheng landslide, the depth of erosion is plotted in Fig 9. In the deposition area, the depth of erosion was less than 1.5 m. Erosion mainly took place in the entrainment area with an average depth value of 2 m. The maximum erosion depth is 4 m at a path distance of about 200 m at the right valley.

In terms of landslide evolution and entrainment, it is essential to highlight the similarities of the present study with the 1998 Cortadonica debris avalanche. In both events, the moving mass bifurcated into two valleys, and the two separated debris avalanches merged again in the deposition zone, to form a single large debris avalanche. In terms of entrainment, the findings of Shuicheng landslide numerical simulation indicate a maximum erosion depth in the middle part of the avalanche run-out path, which also correlates to the conclusion of the literature (Cascini et al. 2011).

Seismic records

Seismic signals of the nearby seismic stations revealed that, on July 23, 2019, an earthquake was detected in Shuicheng, Guizhou, China, with a focal depth of 0 km. However, a high energetic event like the Shuicheng landslide could generate strong seismic signals that were visible above the noise level at 15 three-component broadband seismometers throughout the Guizhou province. Due to the different characteristics and lack of a natural earthquake report of the event area, it can be determined that Shuicheng landslide was the source of those seismic signals.

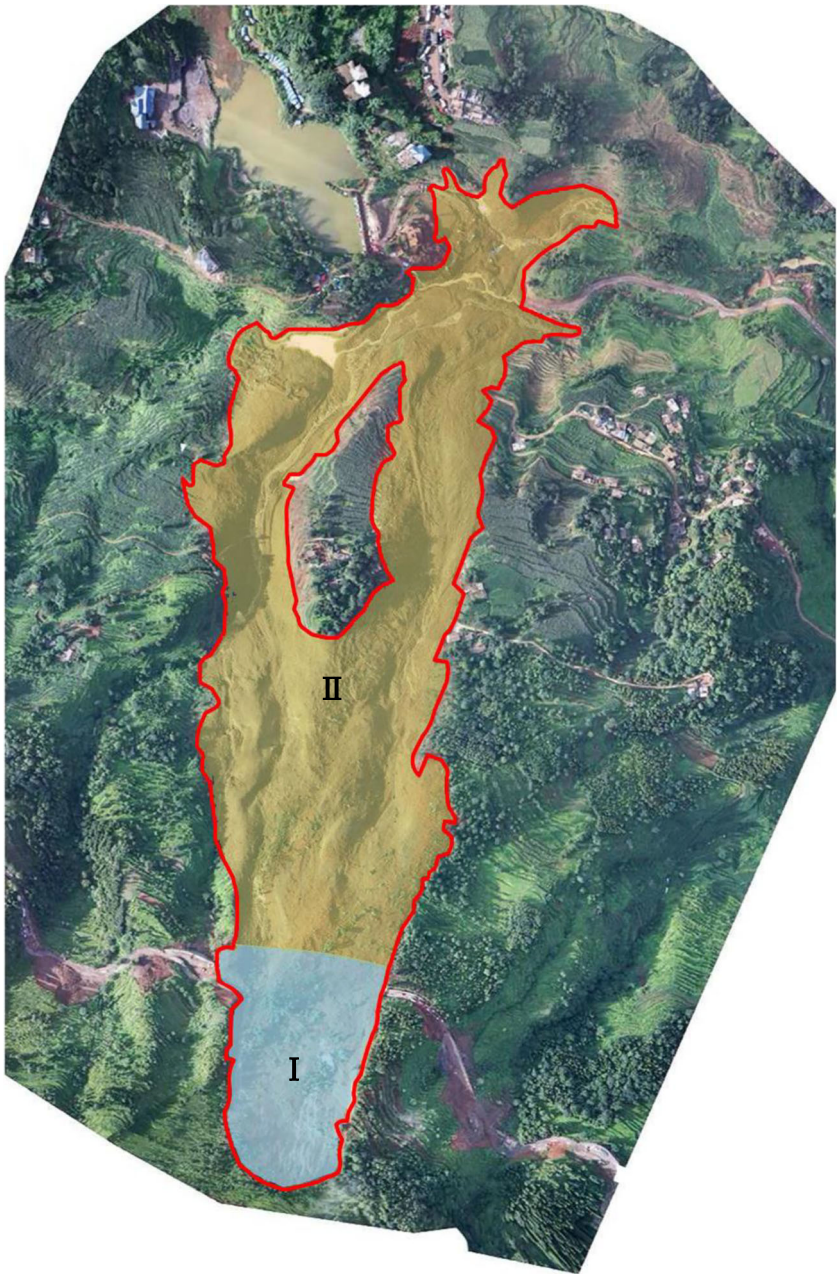

Fig. 6 Outline of the simulation area. I Initiation area. II Entrainment-deposition area

Data and methods

From all the seismic signals available, those with the best signal quality were selected by visual inspection. Seismic signals from twelve stations were used to obtain the location of the event (Fig. 10), while data from YIP station was used to recover the process of the Shuicheng landslide. The seismic stations are shown in relation to the location of the landslide, using google map in Fig. 11 and tabulated details in Table 2.

The intersection method was performed to calculate the location of the event. Assuming seismic station as the center of the circle, while radius as the distance between the seismic station and the calculated location of the event, circles could be drawn based

Table 1 Models and rheological parameters for the Shuicheng landslide

	Rheology	$\phi(^\circ)$	r_u	f	$\xi(m/s^2)$	Maximum erosion depth (m)
Zone I	Frictional	24	0.4	–	–	–
Zone II	Voellmy	–	–	0.2	900	20

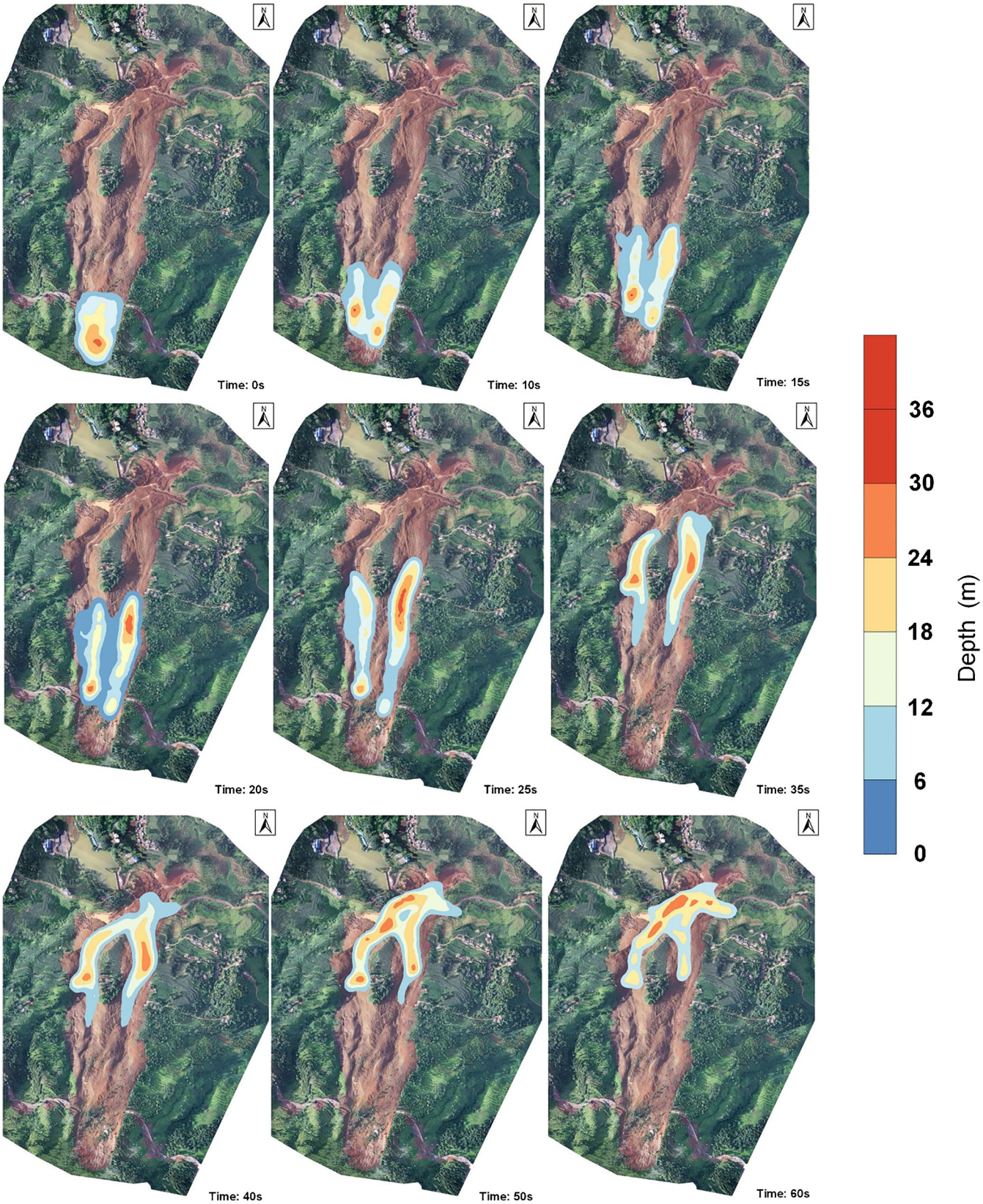

Fig. 7 Evolution of the Shuicheng landslide simulated by DAN3D

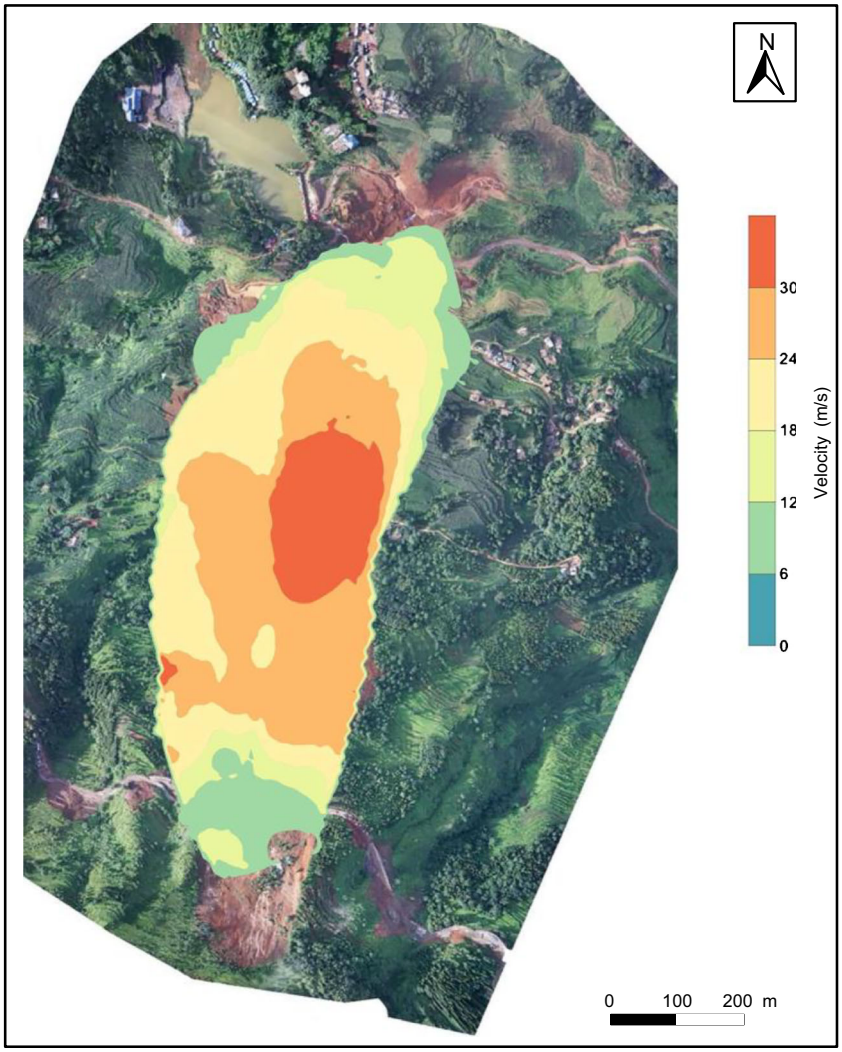

Fig. 8 Maximum velocity contour

on the arriving time difference between the P-wave and S-wave. When the number of stations is greater than three, an approximate intersection can be obtained by the least square method.

Assuming that the focal depth of the landslide is o km, the binary non-linear regression model could be built based on longitudes and latitudes. It is expressed as:

$$t_i = t_o + \frac{d_i}{v_s} + \varepsilon_i \tag{3}$$

where t_i is the time when a seismic station receives seismic signals, t_o is the moment when the event occurs, d_i is the distance between the location of the event and the seismic station, v_s is the velocity of the seismic wave, and ε_i is the random error.

In this study, the Arias intensity was used to describe the variation of kinetic energy (Arias 1970). The governing equation of Arias intensity, I_A, is expressed as:

$$I_A = \frac{\pi}{2g}\int_o^{T_d} a^2(t)dt \tag{4}$$

where $a(t)$ is the acceleration of the seismic signals, T_d is the duration of the seismic signal, and g is the gravitational acceleration.

In order to better understand the pattern of the Arias intensity, the non-dimensionalization method was used by the following equation:

$$I_{A-non} = I_A/(\max I_A) \tag{5}$$

Seismic signals were analyzed by Empirical Mode Decomposition (EMD) method to obtain the intrinsic mode function (IMF). The amplitude-time-frequency spectrum was solved by the Hilbert-Huang transform method (Huang and Wu 2008) to obtain the seismic characteristics of the landslide.

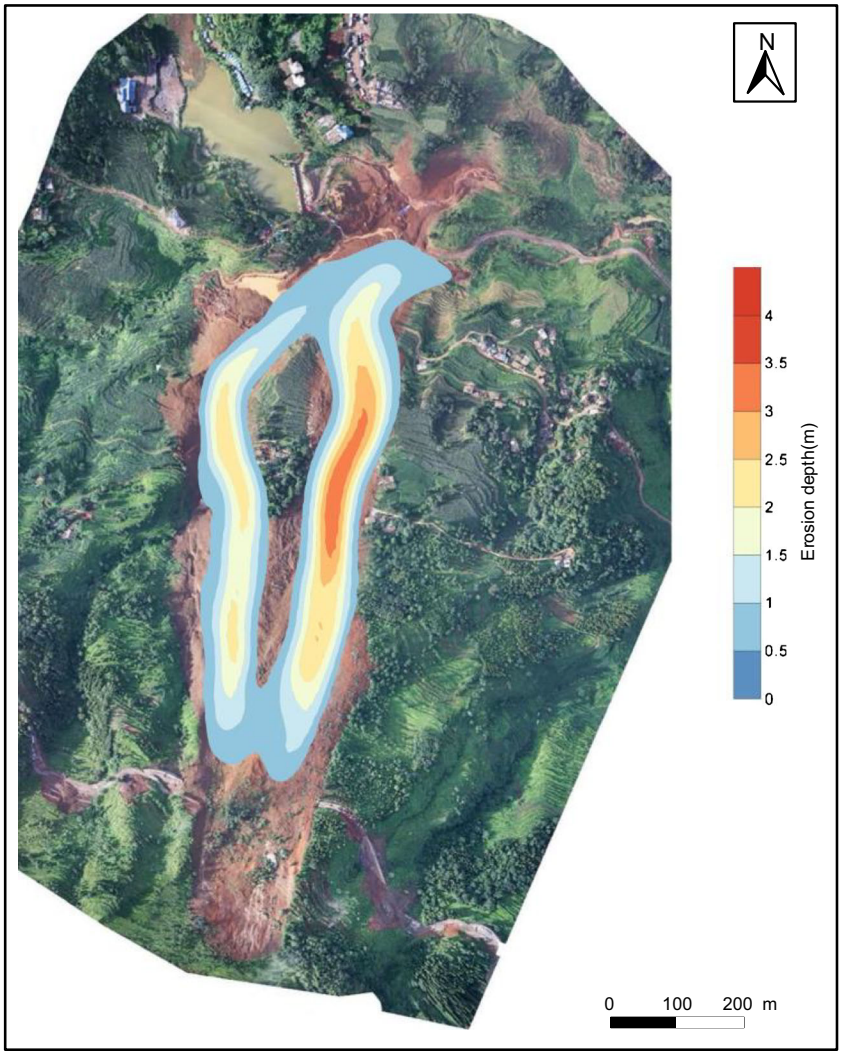

Fig. 9 Erosion depth contour

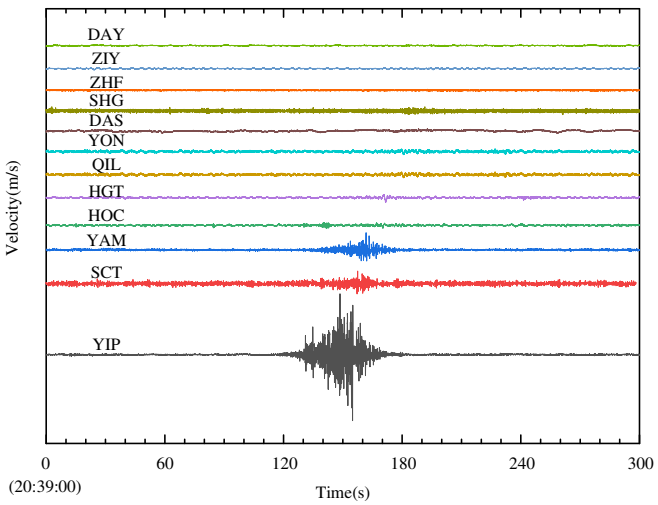

Fig. 10 Seismic signals (vertical component) recorded by near seismic stations

For a landslide of 2 Mm^3 volume, it can be simplified as a block of constant mass sliding down a slope (Fig. 12). Due to gravity and friction, the governing equation of this simplified model is expressed as:

$$F = mg\sin\theta - f \tag{6}$$

where F is the magnitude of the slope parallel force, g is the magnitude of the gravitational acceleration, θ is the slope angle, and f is the frictional force. The magnitude of the frictional force on the block of mass is expressed as:

$$f = N \cdot \mu \tag{7}$$

where μ is the apparent dynamic coefficient of friction, which accounts for both friction and the basal pore fluid pressures, and N is the magnitude of the normal force. The sum of forces in the direction perpendicular to the slope is zero because the landslide

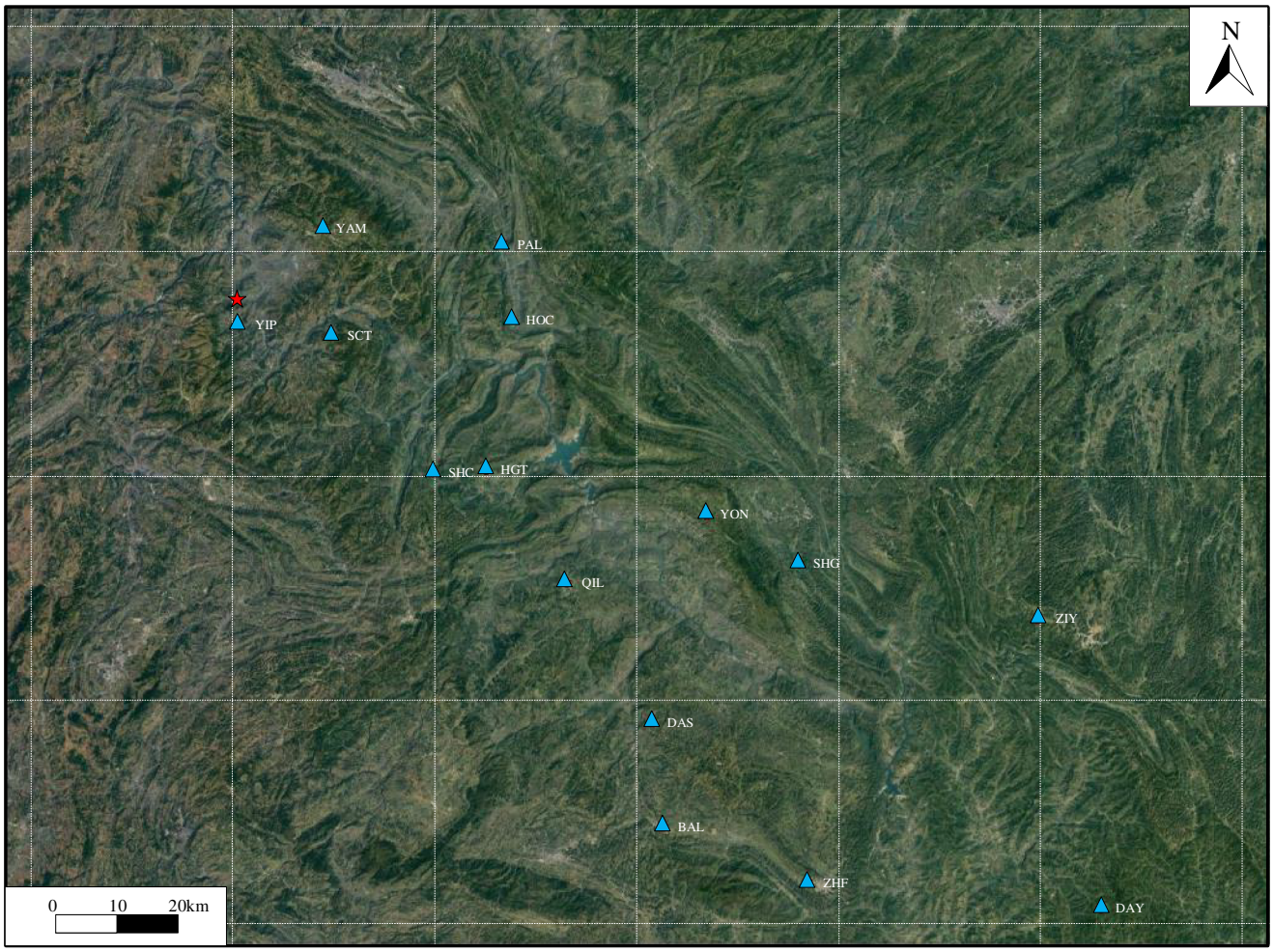

Fig. 11 Locations of the Shuicheng landslide (red star) and seismic stations (blue triangles)

Table 2 Seismic stations used in the inversion

Station name	Longitude/(°)	Latitude/(°)	Distance/km	Source to Station Azimuth/(°)
YIP	104.67	26.22	3.94	179.14
SCT	104.83	26.20	16.72	110.86
YAM	104.82	26.36	18.43	50.50
HOC	105.13	26.23	45.54	93.86
HGT	105.09	26.00	49.89	124.18
QIL	105.22	25.84	71.59	130.38
YON	105.45	25.94	85.41	114.34
DAS	105.36	25.63	97.69	135.19
SHG	105.60	25.87	102.35	114.75
ZHF	105.62	25.39	134.69	135.21
ZIY	106.00	25.78	142.46	111.33
DAY	106.10	25.35	174.61	124.72

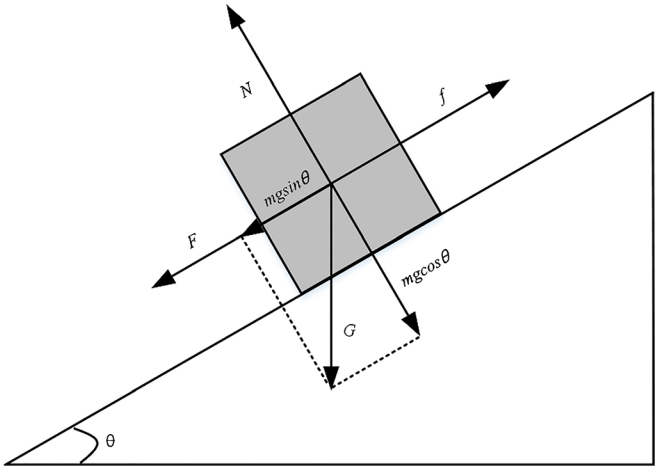

Fig. 12 Schematic diagram illustrating rock avalanche kinematics

moves along the slope and does not accelerate into or out of the slope, so the magnitude of the normal force is equal to:

$$N = mg\cos\theta. \tag{8}$$

This means that the magnitude of the net force F_{net} is equal to the magnitude of the slope parallel force F. In addition, the net force acting on the block is equal to its mass times acceleration, according to Newton's second law. Eq. (6) can be rewritten as:

$$F_{net} = mg(\sin\theta - \mu\cos\theta) = ma \tag{9}$$

where a is the acceleration of the moving mass. Then, the force on the Earth's crust, Fe, can be obtained due to Newton's third law:

$$F_e(t) = -ma(t). \tag{10}$$

Two assumptions were made to invert the force-time function. Rather than the double-couple mechanism of earthquakes, the single force model is applied to the Earth's surface (Kawakatsu 1989; Fukao 1995). It is assumed that the mass of the moving block is constant. Then, the displacement information (U) recorded by seismic stations can be calculated by the convolution of the force-time function with the Green's function (G):

$$U(t) = Fe(t)*G(t)*I(t) \tag{11}$$

where $I(t)$ is the station response. Then, Fe can be solved by using a discrete wave number Green's function (Zhu and Rivera 2002).

Seismic record results

As it is shown in Fig. 13, the distance between the location of the event and different stations was calculated by the intersection method, and the results were processed by the least square method. The event was located at latitude 26°13′6.91″N and longitude

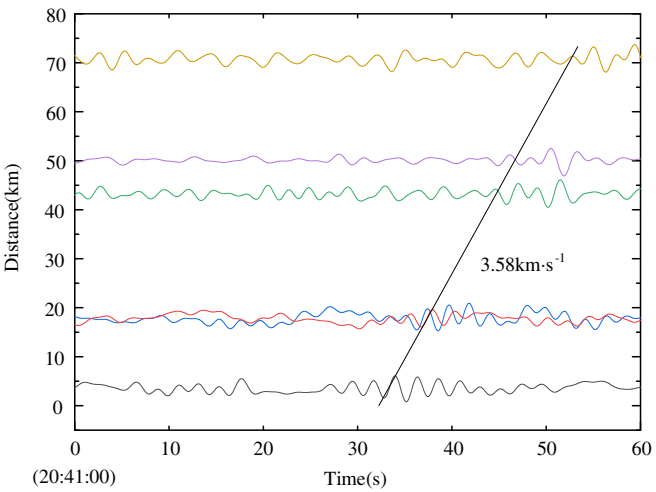

Fig. 13 0.01 ~ 0.1 Hz band-pass filtered seismic signals (vertical component)

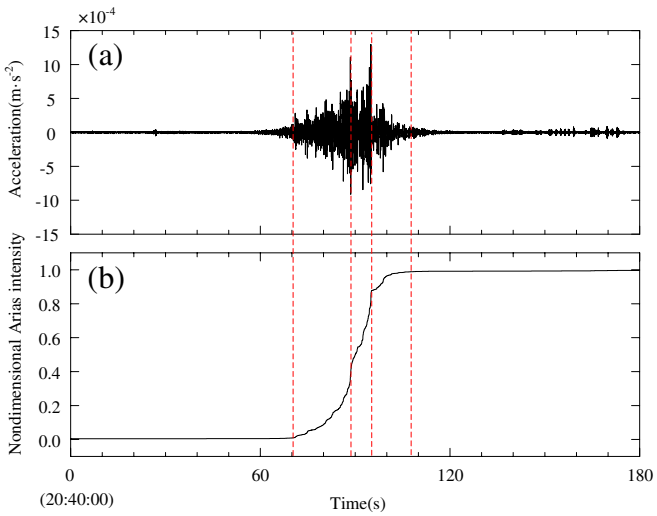

Fig. 14 The intensity of the strong motion in UD direction (YIP)

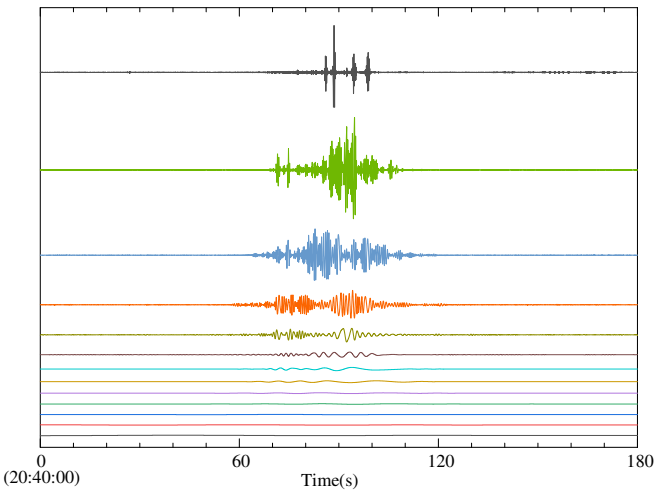

Fig. 15 IMFs 1–13 of the velocity in UD direction from the YIP station

104°40′52.32″E, and results are in good agreement with the location of the landslide. The velocity of the surface wave between the monitoring stations and the location of the event is around 3.58 km/s.

According to the result of the Arias intensity, in Fig 14(a), the peak acceleration was approximately 13×10^{-4} m/s^2, and it lasted about 38 s. In Fig 14(b), before 70 s on the time scale, the change of Arias intensity was negligible. It is noted that the rate of the Arias intensity slope slowed down twice, at 88 s and 95 s. It is deduced that the first slump was at 88 s when the sliding mass collided with the basaltic ridge at an elevation of 1450 m. The second drop was at 95 s when the left branch of the separated sliding mass collided with the outer boundary of the valley and changed its run-out direction. However, there was no considerable change in the Arias intensity when the separated sliding mass collided and merged. The reason is that there was no impact force on the ground surface when the separated mass rammed into each other.

IMFs (Fig. 15) and the amplitude-time-frequency image (Fig. 16) were obtained through the Hilbert-Huang transform. In Fig. 16, high-frequency energy signal was shown during 60 to 80 s, and maintained a maximum level at 70 to 108 s. As shown in the image, there is an increase in the signal twice, from 70 to 81 s and 81 to 108 s. The low-frequency signal reached its peak during 90 to 95 s. High-frequency signal bottoms out from 108 to 120 s and then disappears from background noise after 120 s.

The following conclusions were obtained through the amplitude-time-frequency Hilbert-Huang spectrum image. At 10 s after the initiation of the landslide, the detached mass has divided into parts. After 10 s, the moving mass entrained a large amount of pre-existing loose deposits. At 21 s, the moving mass transformed into a debris avalanche. Combined with the field investigation, it can be deduced that the moving mass collided with the basaltic ridge at an elevation around 1450 m and divided into two branches. The two pre-existing valleys provided the moving mass with distinctive paths and entrainment material. Starting from 30 till 35 s, two separated branches of the same debris avalanche collided and combined at the deposition area, which lies just below those two valleys. From 48 to 60 s, the motion of the debris avalanche was relatively slow and but it continued to accumulate mass. Eventually, the moving mass came to a stop at the deposition area.

The different layered velocity models were calculated on different paths between the monitoring stations, as shown in Table 3. The estimated force-time functions were obtained through the

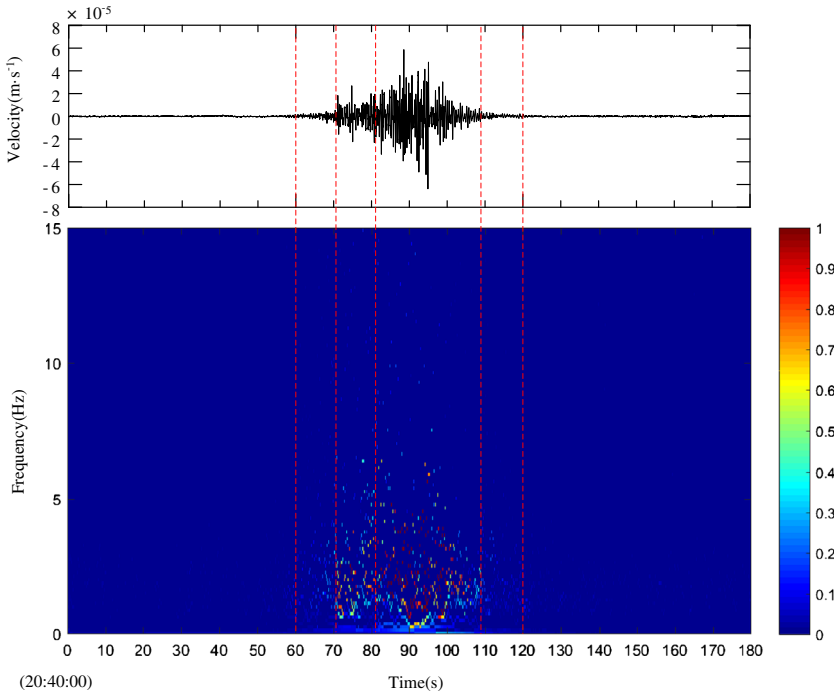

Fig. 16 The amplitude-time-frequency Hilbert spectrum

Table 3 The layered velocity models

Layer	Vp (km/s)	Vs (km/s)	ρ (g/cm)	Depth (km)	μ (GPa)	λ (GPa)	E (GPa)	υ
1	2.5	1.07	2.11	1	2.416	8.356	6.705	0.388
2	4.6	2.59	2.46	4	16.502	19.05	41.846	0.268
3	5	2.88	2.54	1	21.068	21.364	52.743	0.252
4	6.1	3.55	2.74	17.99	34.531	32.894	85.908	0.244
5	6.3	3.65	2.78	15.94	37.037	36.265	92.396	0.247
6	7	3.99	2.95	6.94	46.964	50.621	118.291	0.259

deconvolution of Eq. (11), as it is shown in Fig. 17. No visible pattern appears on the image. In order to validate the result of the force-time functions, we calculated the synthetic seismic signals by the convolution of the obtained force-time and Green's function (Fig. 18). The results show that the synthetic seismic signals and recorded seismic signals are not in agreement with each other. It is deduced that the long-period seismic wave could not be separated from the background noise, leading to the instability of the deconvolution.

Conclusions

On July 23, 2019, a large catastrophic landslide occurred in Shuicheng, Guizhou, China. The Shuicheng landslide was a rapid and long run-out landslide that caused 43 deaths and another nine missing. The displaced material traveled approximately 1250 m and descended approximately 465 m in height. The initial velocity of the slide mass is approximately 24 m/s. After colliding with the basaltic ridge at an elevation of 1450 m, the slide mass transformed into two separated debris avalanches eroding and entraining along the left and right valleys. The two separated branches of debris avalanche collided, merged, and stopped at the deposition area.

In this paper, the propagation and run-out behavior of the Shuicheng landslide were analyzed based on the DAN3D numerical simulation and the seismic signals recorded from the nearby seismic stations. Conclusions are made as follows:

(1) The occurrence of the Shuicheng landslide is closely related to rock mechanical, geological, environmental conditions, and human activities. The main factor of triggering the Shuicheng landslide is heavy rainfall.
(2) The DAN3D model was used to simulate the run-out process, and results showed that a combined Frictional-Voellmy model provides the best performance in simulating the Shuicheng landslide. The total duration of the landslide was 60 s with an average velocity of 20 m/s. A high initial velocity of 24 m/s was recorded at the initiation of the landslide, while the maximum velocity is estimated to be 40 m/s along the right valley adjacent to the basaltic ridge.
(3) The seismic signals recorded by the nearby seismic stations were analyzed to calculate the location of the event and then interpret the run-out process of the Shuicheng landslide. Combining the results of the Arias intensity and Hilbert-

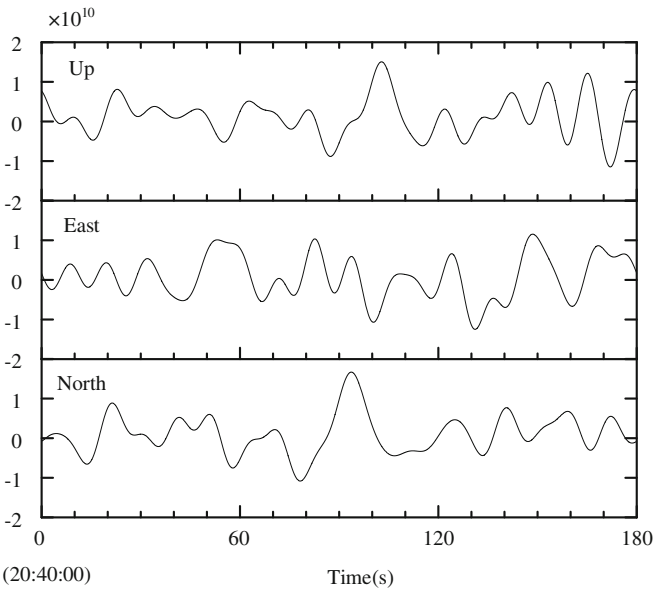

Fig. 17 The force-time function for the Shuicheng landslide

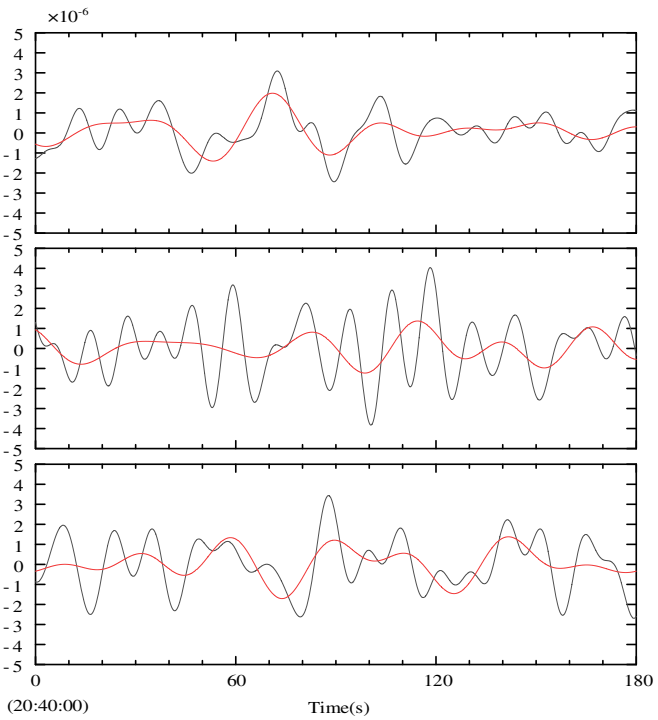

Fig. 18 Synthetic (redlines) and recorded (blacklines) seismic signals

Huang transform with the numerical simulation, a detailed time history of the Shuicheng landslide was obtained. The Shuicheng landslide had a duration of 60 s, comprised of three stages: the initial stage lasted for 10 s, the second stage was between 10 and 48 s, and the third stage had a time duration of 12 s. In the initial stage, the sliding mass detached from the source area with an initial velocity of 24 m/s and collided with the basaltic ridge at an elevation of 1450 m. The second stage lasted 38 s. It started when the sliding mass transformed into two branches around the basaltic ridge, entraining material along the two valleys. The third stage began at 48 s after the initiation of the landslide when the two separated debris avalanches collided and merged into each other. Solved by deconvolution of the displacement function with the Green's function, the force-time functions appeared to be unstable due to the background noise. A comparative analysis between the synthetic and recorded seismic signals was conducted to verify the inaccurate behavior of the force-time function.

Funding information

This study was supported by the National Key R&D Program of China (2018YFC1504804) and the National Natural Science Foundation of China (No. 41977215).

References

Allstadt K (2013) Extracting source characteristics and dynamics of the August 2010 Mount Meager landslide from broadband seismograms. Journal of Geophysical Research:Earth Surface, 2013 118(3):1472–1490

Arias A (1970) A measure of earthquake intensity. In: Hansen RJ (ed) Seismic design for nuclear power plants, vol 1970. MIT Press, Cambridge, Massachusetts, pp 438–483

Bai X, Jian J, He S, Liu W (2019) Dynamic process of the massive Xinmo landslide, Sichuan (China), from joint seismic signal and morphodynamic analyses. Bull Eng Geol Environ. 78(5):3269–3279. https://doi.org/10.1007/s10064-018-1360-0

Cascini L, Cuomo S, De Santis A (2011) Numerical modelling of the December 1999 Cervinara flow-like mass movements (Southern Italy). In: International Conference on Debris-Flow Hazards Mitigation: Mechanics, Prediction, and Assessment, Proceedings, (December 1999), pp 635–644. https://doi.org/10.4408/IJEGE.2011-03.B-069

Cascini L, Cuomo S, Pastor M, Rendina I (2016) SPH-FDM propagation and pore water pressure modelling for debris flows in flume tests. Engineering Geology 213:74–83

Chigira M, Wu X, Inokuchi T, Wang G (2010) Landslides induced by the 2008 Wenchuan earthquake, Sichuan, China. Geomorphology 118(3–4):225–238. https://doi.org/10.1016/j.geomorph.2010.01.003

Coe JA, Baum RL, Allstadt KE, Kochevar BF Jr, Schmitt RG, Morgan ML, White JL, Stratton BT, Hayashi TA, Kean JW (2016) Rock-avalanche dynamics revealed by large-scale field mapping and seismic signals at a highly mobile avalanche in the West Salt Creek valley, western Colorado. Geosphere. 12(2):607–631. https://doi.org/10.1130/GES01265.1

Cuomo S, Pastor M, Capobianco V, Cascini L (2016) Modelling the space–time evolution of bed entrainment for flow-like landslides. Engineering Geology 212:10–20. https://doi.org/10.1016/j.enggeo.2016.07.011

Dai Z, Wang F, Huang Y, Song K, Iio A (2016) SPH-based numerical modeling for the post-failure behavior of the landslides triggered by the 2016 Kumamoto earthquake. Geoenvironmental Disasters 2016:3(1). https://doi.org/10.1186/s40677-016-0058-5

Denlinger RP, Iverson RM (2004) Granular avalanches across irregular three-dimensional terrain: 1. Theory and computation. Journal of Geophysical Research: Earth Surface 109(F1):1–14

Fukao K (1995) Single force representation of earthquakes due to land- slides or the collapse of caverns. Geophys. J. Int. 122:243–248

Helmstetter A, Garambois S (2010) Seismic monitoring of Schilienne rockslide (French Alps): analyses of seismic signals and their correlation with rainfalls. J Geophys Res Earth Surf. 115(3):1–15. https://doi.org/10.1029/2009JF001532

Huang NE, Wu Z (2008) A review on Hilbert-Huang transform: method and its applications. Rev Geophys 46(2007):1–23. https://doi.org/10.1029/2007RG000228.1.INTRODUCTION

Hungr O (1995) A model for the run-out analyses of rapid flow slides, debris flows, and avalanches. Can Geotech J 32(4):610–623

Hungr O, McDougall S (2009) Two numerical models for landslide dynamic analyses. Computers & Geosciences 35:978–992

Hungr O, McDougall S, Bovis M (2005) Entrainment of material by debris flows. In: Debris-flow Hazards and Related Phenomena. Springer Praxis Books. Springer, Berlin, Heidelberg https://doi.org/10.1007/3-540-27129-5_7

Kawakatsu H (1989) Centroid single force inversion of seismic waves generated by landslides. J Geophys Res 94(B9):12, 363–12, 374

Leprettre B, Navarre JP, Taillefer A (1996) First results from a pre-operational system for automatic detection and recognition of seismic signals associated with avalanches. J Glaciol. 42(141):352–363. https://doi.org/10.1017/S0022143000004202

Leprettre B, Navarre JP, Panel JM, Touvier F, Taillefer A, Roulle J (1998) Prototype for operational seismic detection of natural avalanches. Ann Glaciol. 26(1):313–318. https://doi.org/10.3189/1998aog26-1-313-318

Li B, Xing A, Xu C (2017) Simulation of a long-runout rock avalanche triggered by the Lushan earthquake in the Tangjia Valley, Tianquan, Sichuan, China. Eng Geol. 218:107–116. https://doi.org/10.1016/j.enggeo.2017.01.007

Liu W, He S, Li X (2015) Numerical simulation of landslide over erodible surface. Geoenvironmental Disasters 2015:2(1). https://doi.org/10.1186/s40677-015-0027-4

McDougall S, Hungr O (2004) A model for the analyses of rapid landslide motion across three-dimensional terrain. Can Geotech J 41(6):1084–1097

McDougall S, Hungr O (2005) Dynamic modelling of entrainment in rapid landslides. Can Geotech J 42(5):1437–1448

Moran SC, Matoza RS, Garcés MA, Hedlin MAH, Bowers D, Scott WE, Sherrod DR, Vallance JW (2008) Seismic and acoustic recordings of an unusually large rockfall at Mount St. Helens, Washington. Geophys Res Lett. 35(19):2–7. https://doi.org/10.1029/2008GL035176

Moretti L, Allstadt K, Mangeney A et al (2015) Numerical modeling of the Mount Meager landslide constrained by its force history derived from seismic data. J Geophys Res: Solid Earth, 2015 120(4):2579–2599

Navarre JP, Bourova E, Roulle J, Deliot Y (2009) The seismic detection of avalanches: an information tool for the avalanche forecaster. ISSW 09 - Int Snow Sci Work Proc. January:379–383

Pastor M, Quecedo M, Fernández Merodo JA, Herrores MI, Gonzalez E, Mira P (2002) Modelling tailings dams and mine waste dumps failures. Geotechnique 52(8):579–591

Pastor M, Haddad B, Sorbino G, Cuomo S, Drempetic V (2009) A depth-integrated, coupled SPH model for flow-like landslides and related phenomena. International Journal for numerical and analytical methods in geomechanics 33(2):143–172

Pastor M, Yague A, Stickle MM, Manzanal D, Mira P (2018) A two-phase SPH model for debris flow propagation. International Journal for Numerical and Analytical Methods in Geomechanics 42(3):418–448

Quan Luna B, Blahut J, van Asch T, van Westen C, Kappes M (2016) ASCHFLOW - a dynamic landslide run-out model for medium scale hazard analyses. Geoenvironmental Disasters. 2016;3(1). doi:https://doi.org/10.1186/s40677-016-0064-7

Rubin MJ, Camp T, Van Herwijnen A, Schweizer J (2012) Automatically detecting avalanche events in passive seismic data. Proc - 2012 11th Int Conf Mach Learn Appl ICMLA 2012. 1:13-20. doi:10.1109/ICMLA. 2012.12

Sassa K (1988) Geotechnical model for the motion of landslides. In: Proc. 5th International Symposium on Landslides, "Landslides", Balkema, Rotterdam, vol 1, pp 37–56

Van Herwijnen A, Schweizer J (2011a) Monitoring avalanche activity using a seismic sensor. Cold Reg Sci Technol. 69(2-3):165–176. https://doi.org/10.1016/j.coldregions.06.008

Van Herwijnen A, Schweizer J (2011b) Seismic sensor array for monitoring an avalanche start zone: design, deployment and preliminary results. J Glaciol. 57(202):267–276. https://doi.org/10.3189/002214311796405933

Vilajosana I, Suriñach E, Abellán A, Khazaradze G, Garcia D, Llosa J (2008) Rockfall induced seismic signals: case study in Montserrat, Catalonia. Nat Hazards Earth Syst Sci. 8(4):805–812. https://doi.org/10.5194/nhess-8-805-2008

Ward SN, Day S (2006) Particulate kinematic simulations of debris avalanches: interpretation of deposits and landslide seismic signals of Mount Saint Helens, 1980 May 18. Geophys J Int. 167(2):991–1004. https://doi.org/10.1111/j.1365-246X.2006.03118.x

Xing AG, Wang GH, Li B, Jiang Y, Feng Z, Kamai T (2015) Long run-out mechanism and landsliding behaviour of a large catastrophic landslide triggered by a heavy rainfall in Guanling, Guizhou. China. Can. Geotech. J. 52:971–981

Xing A, Xu Q, Zhu Y, Zhu J, Jiang Y (2016) The August 27, 2014, rock avalanche and related impulse water waves in Fuquan, Guizhou, China. Landslides 13(2):411–422. https://doi.org/10.1007/s10346-016-0679-5

Xu Q, Fan X, Huang RQ, Yin Y, Hou S, Dong X, Tang M (2010) A catastrophic rockslide-debris flow in Wulong, Chongqing, China in 2009: background, characterization, and causes. Landslides 7(1):75–87. https://doi.org/10.1007/s10346-009-0179-y

Yamada M, Kumagai H, Matsushi Y, Matsuzawa T (2013) Dynamic landslide processes revealed by broadband seismic records. Geophys Res Lett. 40(12):2998–3002. https://doi.org/10.1002/grl.50437

Yin Y, Xing A (2012) Aerodynamic modeling of the Yigong gigantic rock slide-debris avalanche, Tibet, China. Bulletin of Engineering Geology and the Environment 71(1):149–160. https://doi.org/10.1007/s10064-011-0348-9

Zhu L, Rivera L (2002) A note on the dynamic and static displacements from a point source in multilayered media. Geophys J Int 148:619–627

Zhu Y, Xu S, Zhuang Y, Dai X, Lv G, Xing A (2019) Characteristics and run-out behaviour of the disastrous August 28 2017 rock avalanche in Nayong, Guizhou, China. Eng Geol 259(August 2017):105154. https://doi.org/10.1016/j.enggeo.2019.105154

Y. Zhang · A. Xing (✉) · K. Jin · Y. Zhuang · M. Bilal · S. Xu
State Key Laboratory of Ocean Engineering,
Shanghai Jiao Tong University,
Shanghai, 200240, China
Email: xingaiguo@sjtu.edu.cn

Y. Zhu
State Key Laboratory of Geohazard Prevention and Geoenvironment Protection,
Chengdu University of Technology,
Chengdu, 610059, China

Y. Zhu
Guizhou Institute of Geo-Environment Monitoring,
Guiyang, 550004, Guizhou, China